Using Quasi-continuous Histograms for Fuzzy Main Motion Estimation in Video Sequence

Frédéric Comby, Olivier Strauss

PROD. TYPE: FTP
PP: 1-21 (col.fig.: nil)
FSS4896 MODC+
ED: Bibhu
PAGN: Vish – SCAN: Manjula
ARTICLE IN PRESS
Available online at www.sciencedirect.com
ScienceDirect
Fuzzy Sets and Systems ▮▮▮ (▮▮▮▮) ▮▮▮–▮▮▮
FUZZY sets and systems
www.elsevier.com/locate/fss

Using quasi-continuous histograms for fuzzy main motion estimation in video sequence

F. Comby*, O. Strauss

LIRMM, 161 rue Ada, 34392 Montpellier cedex 5, France

Received 10 March 2005; received in revised form 21 April 2006; accepted 14 September 2006

Abstract

This paper presents a new fuzzy framework for main motion estimation in video sequences. The estimation is performed using a fuzzy representation of pixel gray levels. The motion is characterized by a set of parameters such as horizontal translation, rotation, etc. The method is based on a Hough-like vote procedure. In this scheme, the parametric space is discretized and each pixel votes for each bin of this discrete space. The votes are accumulated in a "quasi-continuous histogram" (QCH). The use of possibility theory and imprecise probabilities provides an accurate estimation of the histogram's mode related to the main motion. The advantages of quasi-continuous histograms in terms of accuracy and robustness are discussed in this paper. Very promising results were obtained using real and simulated video sequences. Comparative studies with classical methods are also presented.

Keywords: Main apparent motion; Image processing; Fuzzy; Possibility theory; Imprecision; Uncertainty; Quasi-continuous histograms

1. Introduction

When a digital camera moves in an almost static scene, the retina illumination distribution is coherently modified. This modification, called "global apparent motion'', is achieved by a displacement of the projection of the environment objects on the focal plane. Major changes in the image sequence are generally due to camera operation and motion. However, phenomena such as occlusion, moving objects or global illumination variations can also generate, or be interpreted as, apparent motion. The idea of global motion is then replaced by the main motion concept, where "main'' stands for the motion associated with the largest number of pixels.

Main motion estimation in a video sequence addresses the problem of computation of main image transformation over time. This is a key issue in image processing and computer vision. It has many applications, for example, in object tracking [28,22], estimation of a mobile robot's egomotion [6], mosaicing [19,33,29] and motion stabilization.

At first sight, recovering apparent motion between two shots via the intensity variation is impossible because each pixel of the image has two degrees of freedom while only one information element is available (intensity variation). Consequently, hypotheses have to be put forward about a supposed regularity of the scene. A so called "regularization technique'' may then be used. For example, if all objects of the scene are far enough from the camera, then they seem to belong to the same global plane [47]. The six degrees of freedom movement of the camera produces an apparent

* Corresponding author. Tel.: +33 0 4 67 41 85 87; fax: +33 0 4 67 41 85 00.
E-mail addresses: comby@lirmm.fr (F. Comby), strauss@lirmm.fr (O. Strauss).

0165-0114/$ - see front matter © 2006 Elsevier B.V. All rights reserved.
doi:10.1016/j.fss.2006.09.011

Please cite this article as: F. Comby, O. Strauss, Using quasi-continuous histograms for fuzzy main motion estimation in video sequence, Fuzzy Sets and Systems (2006), doi: 10.1016/j.fss.2006.09.011

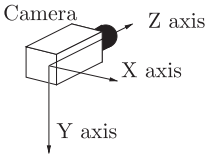

Fig. 1. Camera frame axes.

motion that can be approximated by a six degrees of freedom model [20]. This model, called an affine model, appears to be suitable for many applications, especially when there is very little camera movement between two consecutive images.

The complexity of the global motion model used is related to the accuracy of the motion description, but also to the computational complexity and stability [31]. A sophisticated model can be chosen to match the sought-after apparent motion more closely, but its robustness (sensitivity to outliers) is generally very low. Main motion estimation thus requires robust statistics. In this contribution, we present a very new robust parametric estimator able to overcome many flaws of common main movement estimators. We do not focus on any particular model. To simplify the explanations and illustrations, we will thus focus on a simple three parameter motion model (two translations along the X and Y axis and a rotation around the Z axis, see Fig. 1). However, the method can be used with many more complex motion models (see Section 4.3).

The aim of this paper is not to present a new evolution of classical motion estimator. We only intend to present a new framework, a new way to grasp the motion estimation problem. This paper is organized as follows: Section 2 briefly presents previous work on motion estimation. Section 3 introduces the quasi-continuous histogram (QCH) as an modal estimation technique. Section 4 presents the motion estimation algorithm. Eventually, in Section 5 we discuss some results and compare our approach with some state of art methods. We will conclude on the beneficial features of this methodology and highlight its potential.

2. Previous work

Classical methods for motion estimation can be mostly divided into three categories: feature-based, correlation-based and gradient-based methods [26]. Feature-based methods seem to be ill-adapted to main motion estimation since features represent sparse areas in the image which movement is unlikely linked to main motion. They are highly sensitive to ambiguity among the structures to be matched. This aspect will not be furtherly discussed in this paper.

2.1. Correlation-based methods

Correlation-based techniques, also known as window-matching ones are the most intuitive to perform motion estimation. They are based on analyzing the gray level pattern (reference pattern) and searching the most similar pattern in the successive image (tested pattern). They assume that the pattern gray-level distribution does not change too much between two consecutive images and that the texture is significant enough to correctly match the patterns. The difference between the pattern positions in two consecutive images is related to the motion. Thus, correlation-based methods involve finding the "best" 2-D-transformation or 2-D-motion between two images. These techniques typically assume that the sought-after transformation belongs to a known parametrized motion model. Table 1 presents the three usual basic models: translational, affine, quadratic. A combination of the three can also be used.

The estimation of this transformation involves a discretization of the parameter space and the use of a statistical similarity measure. Each combination of the parametric space is evaluated through a distance (or a similarity measure) between the intensity patterns. The value of the parameter that maximizes the similarity measure (or minimizes the distance) is assigned to main motion. The main algorithms are detailed in Table 2, where $I_1(i, j)_{i\in[1,M],j\in[1,N]}$ stands for the gray level located at (i, j) coordinates on the $M \times N$ reference pattern (on I_1 image); the tested pattern is on image I_2; (u, v) is the motion evaluated (in pixels) and $\overline{I}$ is the mean intensity of image I.

Matching algorithms were first based on standard statistical methods, which are best suited to a single population [35,1]. Considering that parametric measures, such as correlation, euclidean distance, mean or variance do not be-

Please cite this article as: F. Comby, O. Strauss, Using quasi-continuous histograms for fuzzy main motion estimation in video sequence, Fuzzy Sets and Systems (2006), doi: 10.1016/j.fss.2006.09.011

Table 1
Classical basic motion models

Translational	$w(p_i) = \begin{pmatrix} c_1 \\ c_2 \end{pmatrix}$
Affine	$w(p_i) = \begin{pmatrix} a_1 & a_2 \\ a_3 & a_4 \end{pmatrix} \begin{pmatrix} x_i \\ y_i \end{pmatrix}$
Quadratic	$w(p_i) = \begin{pmatrix} q_1 & q_2 & q_3 \\ q_4 & q_5 & q_6 \end{pmatrix} \begin{pmatrix} {x_i}^2 \\ x_i y_i \\ {y_i}^2 \end{pmatrix}$

$w(p_i) = (u(p_i), v(p_i))^t$ stands for the flow vector at point $p_i = (x_i, y_i)^t$ (motion on the image).

Table 2
State of art distance measures for an apparent motion (u, v) in the image plane between images I_1 and I_2

SAD(u,v)	$\sum_{i=1}^{M}\sum_{j=1}^{N} \lvert I_1(i,j) - I_2(i+u, j+v)\rvert$
ZSAD(u,v)	$\sum_{i=1}^{M}\sum_{j=1}^{N} \lvert (I_1(i,j) - \overline{I_1}) - (I_2(i+u, j+v) - \overline{I_2})\rvert$
SSD(u,v)	$\sum_{i=1}^{M}\sum_{j=1}^{N} (I_1(i,j) - I_2(i+u, j+v))^2$
ZSSD(u,v)	$\sum_{i=1}^{M}\sum_{j=1}^{N} ((I_1(i,j) - \overline{I_1}) - (I_2(i+u, j+v) - \overline{I_2}))^2$
NCC(u,v)	$\frac{\sum_{i=1}^{M}\sum_{j=1}^{N} I_1(i,j) I_2(i+u,j+v)}{\sqrt{\sum_{i=1}^{M}\sum_{j=1}^{N} I_1^2(i,j) I_2^2(i+u,j+v)}}$
ZNCC(u,v)	$\frac{\sum_{i=1}^{M}\sum_{j=1}^{N} (I_1(i,j)-\overline{I_1})(I_2(i+u,j+v)-\overline{I_2})}{\sqrt{\sum_{i=1}^{M}\sum_{j=1}^{N} (I_1(i,j)-\overline{I_1})^2 (I_2(i+u,j+v)-\overline{I_2})^2}}$

SAD stands for Sum of Absolute Difference, SSD for Sum of Squared Difference and their zero-centered version: ZSAD and ZSSD, where the pattern mean intensity is subtracted. Subtracting the mean intensity decreases the sensitivity to a global illumination variation. A similarity measure NCC (Normalized Cross Correlation) and ZNCC its zero-centered version are also detailed. i and j are indexes to roam the images.

have well in the presence of distinct sub-populations, non-parametric statistical tools have been used to deal with this matter [46,3,5]. Non-parametric statistics involve ordering information in data sets, while parametric statistics use the data directly. Non-parametric methods involve a transformation of the gray-level patterns. The two main transformation used in correlation-based methods are presented here: Rank and Census transforms. Rank transform [46] replace each pixel gray level value by its rank in gray level ascending order within the pattern (or the whole image). Then classical methods such as SAD, SSD perform similarity measure on the Rank-transformed images. Census transform [46] uses a reference pixel in the pattern (usually the center of the pattern). Each pixel gray level of the pattern is replaced by a boolean value indicating whether its gray level is bigger than the reference one. The Census-transformed image is thus a bit chain composed of zeros and ones. The similarity between the two boolean chains is performed with a Hamming distance (the sum of all digits of an *exclusive or* (*XOR*) between the two Census-transformed patterns).

The use of rank statistics improves the robustness of the estimation process for illumination changes. However, these methods are only well suited for integer translational displacement. Rotations, distortions or scaling introducing non-integer displacement are generally badly estimated. Parameter space discretization is one of the major drawbacks of this kind of methods because the estimation precision is limited by the parameter space sampling interval. Besides, this discretization is highly arbitrary and its effect on imprecision is generally not considered. A thorough study of these techniques and their improvements can be found in [18].

Please cite this article as: F. Comby, O. Strauss, Using quasi-continuous histograms for fuzzy main motion estimation in video sequence, Fuzzy Sets and Systems (2006), doi: 10.1016/j.fss.2006.09.011

2.2. Gradient-based methods

Optical flow-based (OF), or gradient-based methods were introduced by Horn [21] and have been intensively investigated and improved [17,26,30,16,7]. They generally involve computing velocity from first-order derivatives of the image intensity. Let $E(x, y, t)$ be the irradiance image, i.e. the spatio-temporal variation in the illumination on the retina (or focal plane). If image brightness can be considered as invariant along image motion trajectories, and assuming that $E(x, y, t)$ is differentiable, then the velocity (u, v) of the pixel (x, y) at time (t) is constrained by

$$\nabla E_{(x,y)} * (u, v)^{\mathrm{T}} + E_t = \xi, \tag{1}$$

where $\nabla E_{(x,y)}$ is the spatial gradient, and E_t the temporal gradient of the irradiance image; $(u, v)^{\mathrm{T}} = (\mathrm{d}x/\mathrm{d}t, \mathrm{d}y/\mathrm{d}t)^{\mathrm{T}}$ is the projection of the 3-D velocity field in the focal plane, T is the transposition operator, and ξ is the global brightness variation. The so-called "gradient constraint" alone cannot be used to compute optical flow since for each pixel there is only one equation for two unknowns (u, v). The optical flow constraint is therefore usually combined with the assumption that nearby points move the same way. It is also assumed that local continuity provides a regularization process that groups neighboring constraint equations to give a local estimation of velocity [21].

Without a multi-resolution process, only small displacement can be estimated. In [24] the authors were the first to present an iterative process for large displacement estimation. However, as the parameters need to be arbitrarily initialized, the process may converge toward a local solution. A coarse to fine process needs to be added to obtain the global solution.

However, the main problem regarding the gradient-based approaches is that they are based on two antagonistic assumptions [23]. On the one hand, the image must be sufficiently textured for the motion to be seen on the image (if $\nabla E_{(x,y)}$ and E_t are null, no motion can be estimated); on the other hand, the computation of local gradients $\nabla E_{(x,y)}$ and E_t is made through a low-pass filter, which assumes a low image texture. Moreover, the use of discrete filters to compute local gradients involves imprecision which is neglected in the estimation process.

The optical flow hypothesis is mainly based on the idea that the observed brightness is constant over time. Its computation is very sensitive to gradient estimates, local variations (moving objects), noise in the acquisition process and sampling, regularization, etc. Robust statistics have been used extensively to cope with the ill-conditioned assumptions about movement mono-modality and other problems, such as the partial occlusion effect [31,44]. Multi-scale estimation, in a coarse to fine refinement, is generally used for large displacement estimation [25,39]. So far nothing has been proposed to deal with the imprecision induced by filtering.

2.3. Toward a new framework?

A new approach is required to overcome these limitations. It should be as robust as gradient-based approaches using robust statistics with respect to outliers and as robust as correlation-based methods using rank statistics concerning optical flow constraint weaknesses. Rather than offering yet another improvement to existing methods, a new methodology for main apparent motion detection and estimation is presented.

The underlying idea behind our approach is to place the whole correspondence problem within a fuzzy logical frame. This will lower the influence of image gain and bias. It will also improve the robustness regarding the basic assumption of intensity distribution conservation.

As in correlation-based methods, the transformation to be estimated is assumed to belong to a known parametrized motion model. Quantization's effects of the parameter space are taken into account by a new statistical estimator called "quasi-continuous histograms". This technique partly deals with the inherent problem of discrete estimator precision.

3. Quasi-continuous histograms

The concept of main motion in a video sequence is related to the apparent motion of most pixels between two consecutive images. The process described here has many aspects in common with polling Hough-like processes. The Hough transform key concept uses a sampled parametrized model of apparent motion and asks all pixels to "vote" for each parameter value. The main motion is said to be represented by the set of parameters obtaining the highest score.

In a previous article [40], we have demonstrated how to deal with discretization in the polling process. This article introduces a theoretical framework called "quasi-continuous histograms" (QCH), [9]. It is based on the fuzzy rough

Please cite this article as: F. Comby, O. Strauss, Using quasi-continuous histograms for fuzzy main motion estimation in video sequence, Fuzzy Sets and Systems (2006), doi: 10.1016/j.fss.2006.09.011

sets theory [14,32]. The main goal here is to dissociate the histogram's granularity from the precision of the information computed using the histogram. The major drawbacks of classical histograms are linked to the crisp partition of the utilized space. In order to lower arbitrary aspect space partitioning, QCH are built on a fuzzy partition [4] (instead of a crisp one). The advantages of this partition (Fig. 2) will be discussed in Sections 3.1 and 3.2.

The membership function of the kth cell is

$$\mu_{\boldsymbol{h_k}}(x) = \left\{ \begin{array}{ll} \frac{1}{\Delta}(x - e_{\min} - (k-1)\Delta) & \text{if } x \in [e_{\min} + (k-1)\Delta, e_{\min} + k\Delta] \\ 1 - \frac{1}{\Delta}(x - e_{\min} - k\Delta) & \text{if } x \in [e_{\min} + k\Delta, e_{\min} + (k+1)\Delta] \\ 0 & \text{else} \end{array} \right\}, \tag{2}$$

where $x \in \mathbb{R}$, 2Δ is the width of a triangular cell and m_k is the central position of the kth partition interval (i.e. $m_k = e_{\min} + k\Delta$). The triangular membership function has been chosen for the fuzzy partition because it is the most generic membership function to represent mono-modal symmetric fuzzy numbers [12]. Moreover, a strong fuzzy partition (satisfying $\forall(x \in \mathbb{R})$, $\sum_{k=1}^{p} \mu_k(x) = 1$, where p is the number of bins) is needed to perform counting on data accumulated on the histogram. This justifies the shape of the first and last histogram cells.

Let us now introduce some notations that will be used throughout the rest of the document. When the representation of data d is set-theoretic (data is imprecise), it will be noted as bold $\boldsymbol{d}$. When the data $(\boldsymbol{d_i})_{i\in[1,N]}$ are precise, their definition domain is represented by a singleton $\boldsymbol{d_i} = \{d_i\}$ with $\boldsymbol{d_i} \in \mathbb{R}$. When talking about all data (precise or not) $(\boldsymbol{d_i})_{i\in[1,N]}$ we will use $(\boldsymbol{d_i})$ to ease the reading.

3.1. Precise data accumulation

Regarding precise data, the generalization of the classical histogram accumulation process can be expressed as:

$$Acc_k = \sum_{i=1}^{N} mu_{\boldsymbol{h_k}}(d_i) \tag{3}$$

where μ_k is the membership function of the fuzzy subset H_k and N the number of data. This polling scheme amounts to distributing the influence of data on two contiguous fuzzy partition's cells, thus limiting the influence of the class boundaries. This is illustrated in Fig. 3 where Acc_k (resp. Acc_{k+1}) represent the $\boldsymbol{h_k}$ (resp. $\boldsymbol{h_{k+1}}$) accumulator.

Remark 1. As with classical histograms, the relation $\sum_{k=1}^{P} Acc_k = N$, with N being the data number and P the bins number, is still true. Using quasi-continuous histograms does not give rise to uncertainty on the number of votes when the data are precise.

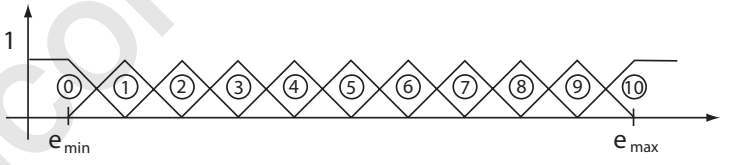

Fig. 2. 11 cells membership functions forming a strong fuzzy partition of the real axis between $e_{\min}$ and $e_{\max}$.

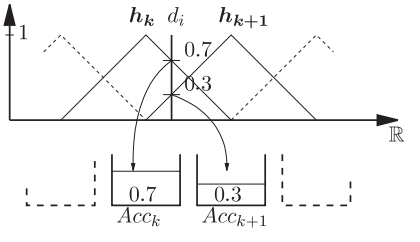

Fig. 3. Precise data votes on a quasi-continuous histogram. This illustrates the data influence range for 2 consecutive cells of the QCH.

Please cite this article as: F. Comby, O. Strauss, Using quasi-continuous histograms for fuzzy main motion estimation in video sequence, Fuzzy Sets and Systems (2006), doi: 10.1016/j.fss.2006.09.011

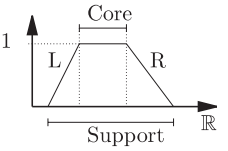

Fig. 4. Fuzzy quantity with its L–R representation.

3.2. Imprecise data accumulation

In physical systems, data are often not precisely known. For example sensors usually provide measures with a given precision. When data $(\boldsymbol{d_i})_{i\in[1,N]}$ are imprecise with a known reference domain, this imprecision can be easily represented by fuzzy quantities (Fig. 4) [43].

In this case, Eq. (3) has to be generalized. $\mu_{\boldsymbol{h_k}}(d_i)$, measuring how much d_i is compatible with the $\boldsymbol{h_k}$ cell, has to be replaced by a measure of compatibility between the two subsets $\boldsymbol{h_k}$ and $\boldsymbol{d_i}$: $M(\boldsymbol{h_k};\boldsymbol{d_i})$. This measure has to evaluate knowledge about $\boldsymbol{d_i}$ when $\boldsymbol{h_k}$ is known. The aim of QCH is to transfer the imprecision of $\boldsymbol{d_i}$ on the knowledge of this compatibility value. The compatibility is then represented by an interval containing all possible values of $M(\boldsymbol{h_k};\boldsymbol{d_i})$ [13,15]. The boundaries of this interval can be computed using possibility theory:

$$\Pi(\boldsymbol{h_k};\boldsymbol{d_i}) = \sup_{\Omega}(\min(\mu_{\boldsymbol{h_k}}(x), \mu_{\boldsymbol{d_i}}(x))), \tag{4}$$

$$N(\boldsymbol{h_k};\boldsymbol{d_i}) = \inf_{\Omega}(\max(\mu_{\boldsymbol{h_k}}(x), 1-\mu_{\boldsymbol{d_i}}(x))), \tag{5}$$

where Ω is the real axis, $\mu_{\boldsymbol{d_i}}$ the membership function of $\boldsymbol{d_i}$, and $\mu_{\boldsymbol{h_k}}$ the membership function of the $\boldsymbol{h_k}$ cell of the fuzzy partition. These boundaries satisfy

$$N(\boldsymbol{h_k};\boldsymbol{d_i}) \leqslant M(\boldsymbol{h_k};\boldsymbol{d_i}) \leqslant \Pi(\boldsymbol{h_k};\boldsymbol{d_i}) \tag{6}$$

and $\Pi(\boldsymbol{h_k};\boldsymbol{d_i})$ defines how $\boldsymbol{d_i}$ intersects the $\boldsymbol{h_k}$ cell, whereas $N(\boldsymbol{h_k};\boldsymbol{d_i})$ defines how $\boldsymbol{d_i}$ is included in $\boldsymbol{h_k}$. Therefore, the generalization of Eq. (3) involves a replacement of the precise accumulator by an imprecise one defined by its two boundaries, called lower ($\underline{Acc_k}$) and upper ($\overline{Acc_k}$) accumulator, as follows:

$$\underline{Acc_k} = \sum_{i=1}^{N} N(\boldsymbol{h_k};\boldsymbol{d_i}), \tag{7}$$

$$\overline{Acc_k} = \sum_{i=1}^{N} \Pi(\boldsymbol{h_k};\boldsymbol{d_i}) \tag{8}$$

If an imprecise data $\boldsymbol{d_i}$ with its membership function $\mu_{\boldsymbol{d_i}}$ has to be accumulated on the QCH, Figs. 5 and 6 illustrate the determination of the two compatibility boundaries between $\boldsymbol{h_k}$ and $\boldsymbol{d_i}$: $N(\boldsymbol{h_k};\boldsymbol{d_i})$ and $\Pi(\boldsymbol{h_k};\boldsymbol{d_i})$.

The gap between the two accumulators is linked to the data imprecision. When data are precise, the gap is nul and the accumulators are identical, since: $\Pi(\boldsymbol{h_k};\boldsymbol{d_i}) = N(\boldsymbol{h_k};\boldsymbol{d_i}) = \mu_{\boldsymbol{h_k}}(\boldsymbol{d_i})$.

Remark 2. In the case of imprecise data, the following relations are satisfied : $\sum_{k=1}^{P} \overline{Acc_k} \geqslant N$, $\sum_{k=1}^{P} \underline{Acc_k} \leqslant N$, where P is the bins number.

3.3. Link with imprecise probabilities

There is a strong link between histogram accumulation and probabilities of the histogram bins [45]. If the data d_i are precise, then $P(\boldsymbol{h_k})$ can be estimated by

$$P(\boldsymbol{h_k}) = \int_{\boldsymbol{h_k}} p(h)\,\mathrm{d}h \approx \frac{Acc_k}{N} = \frac{Nb(\boldsymbol{h_k};(d_i))}{N} \tag{9}$$

Please cite this article as: F. Comby, O. Strauss, Using quasi-continuous histograms for fuzzy main motion estimation in video sequence, Fuzzy Sets and Systems (2006), doi: 10.1016/j.fss.2006.09.011

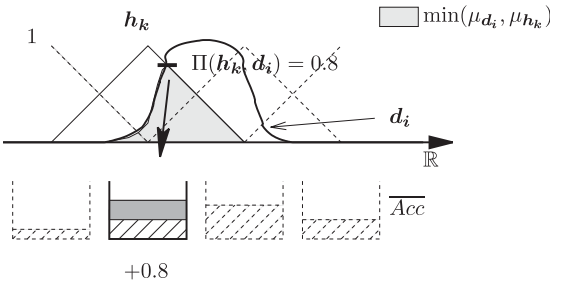

Fig. 5. Illustration of $\Pi(\boldsymbol{h_k}; \boldsymbol{d_i})$ computation (see Eq. (5)). The gray shaded area represents the minimum of $\mu_{d_i}(x)$ and $\mu_{h_k}(x)$ whatever may $x \in \mathbb{R}$ be. $\Pi(\boldsymbol{h_k}; \boldsymbol{d_i})$ stands for the maximum height of this gray shaded area. This value (0.8 in the figure) is accumulated on the upper accumulator associated to $\boldsymbol{h_k}$ bin.

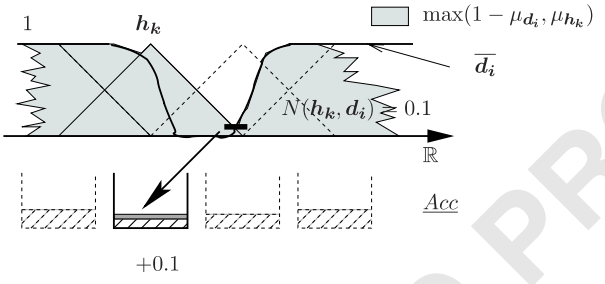

Fig. 6. Illustration of $N(\boldsymbol{h_k}; \boldsymbol{d_i})$ computation (see Eq. (4)). The gray shaded area represents the maximum of $\mu_{\overline{d_i}}(x) = 1 - \mu_{d_i}(x)$ and $\mu_{h_k}(x)$ whatever may $x \in \mathbb{R}$ be. $N(\boldsymbol{h_k}; \boldsymbol{d_i})$ stands for the minimum of the gray shaded area. This value (0.1 in the figure) is accumulated on the lower accumulator associated to $\boldsymbol{h_k}$ bin.

where $P(\boldsymbol{h_k})$ is the occurrence probability of the event $\boldsymbol{h_k}$, $p(f)$ is the probability density function (pdf) of f, $Nb(\boldsymbol{h_k}; (\boldsymbol{d_i}))$ the number of data d_i in $\boldsymbol{h_k}$ and N is the data total number. When data are imprecise, $P(\boldsymbol{h_k})$ is imprecise too. A generalization of Eq. (9) can be given as: $P(\boldsymbol{h_k}; (\boldsymbol{d_i})) \in [\underline{P}(\boldsymbol{h_k}); \overline{P}(\boldsymbol{h_k})]$ with

$$\underline{P}(\boldsymbol{h_k}) = \frac{\underline{Nb}(\boldsymbol{h_k}; (\boldsymbol{d_i}))}{\underline{Nb}(\boldsymbol{h_k}; (\boldsymbol{d_i})) + \sum_{j \neq k} \overline{Nb}(\boldsymbol{h_j}; (\boldsymbol{d_i}))}, \tag{10}$$

$$\overline{P}(\boldsymbol{h_k}) = \frac{\overline{Nb}(\boldsymbol{h_k}; (\boldsymbol{d_i}))}{\overline{Nb}(\boldsymbol{h_k}; (\boldsymbol{d_i})) + \sum_{j \neq k} \underline{Nb}(\boldsymbol{h_j}; (\boldsymbol{d_i}))} \tag{11}$$

and

$$\underline{Nb}(\boldsymbol{h_k}; (\boldsymbol{d_i})) = \sum_{i=1}^{N} N(\boldsymbol{h_k}; \boldsymbol{d_i}), \tag{12}$$

$$\overline{Nb}(\boldsymbol{h_k}; (\boldsymbol{d_i})) = \sum_{i=1}^{N} \Pi(\boldsymbol{h_k}; \boldsymbol{d_i}). \tag{13}$$

3.4. Probability density and pignistic transfer

The most widely used density estimators are classical histograms. If the underlying probability density is assumed to be uniform in a bin $\boldsymbol{h_k}$, then the density of any x belonging to $\boldsymbol{h_k}$ can be ranked as: $p(x) = Acc_k / N\Delta$.

The discontinuity of the density estimation given by classical histograms causes severe difficulties, especially when the density derivative is needed. A continuous estimation of the density function can be estimated via QCH. The method

Please cite this article as: F. Comby, O. Strauss, Using quasi-continuous histograms for fuzzy main motion estimation in video sequence, Fuzzy Sets and Systems (2006), doi: 10.1016/j.fss.2006.09.011

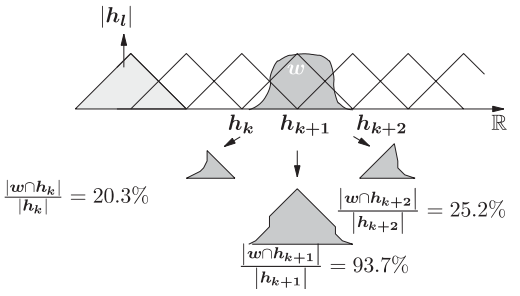

Fig. 7. Illustration of weighting coefficient computation $|\boldsymbol{w} \cap \boldsymbol{h_k}|/|\boldsymbol{h_k}|$ for the histogram votes pignistic transfer toward any subset $\boldsymbol{w}$.

is very close to the so-called kernel method [34]. It involves transferring votes from whole sets of bins to any crisp or fuzzy subset $\boldsymbol{w}$ of $\Omega(\mathbb{R})$ (with $\Omega(\mathbb{R}) = \bigcup_k \boldsymbol{h_k}$) by using the pignistic transfer [36,37]. When the data are precise, this transfer is written

$$Nb(\boldsymbol{w}; (d_i)) = \sum_{k=0}^{p} Acc_k \frac{|\boldsymbol{w} \cap \boldsymbol{h_k}|}{|\boldsymbol{h_k}|}, \tag{14}$$

where p is the number of cells of the partition and $|\boldsymbol{x}|$ is the cardinal of $\boldsymbol{x}$'s membership function. The principle of vote transfer toward any subset $\boldsymbol{w}$ is illustrated in Fig. 7.

When data are imprecise, the estimation of $Nb(\boldsymbol{w}; (\boldsymbol{d_i}))$ is also imprecise and Eq. (14) becomes

$$\underline{Nb}(\boldsymbol{w}; (\boldsymbol{d_i})) = \sum_{k=0}^{p} \underline{Acc_k} \frac{|\boldsymbol{w} \cap \boldsymbol{h_k}|}{|\boldsymbol{h_k}|}, \tag{15}$$

$$\overline{Nb}(\boldsymbol{w}; (\boldsymbol{d_i})) = \sum_{k=0}^{p} \overline{Acc_k} \frac{|\boldsymbol{w} \cap \boldsymbol{h_k}|}{|\boldsymbol{h_k}|}. \tag{16}$$

3.5. Finding a mode at a given resolution

Finding a mode in a sample of n real data involves finding bumps in the underlying density distribution. A very simple histogram-based method has been proposed in [10]. Assuming that neighboring bins are linearly related, Cox uses an estimation of the first derivative of the underlying density to provide some informal evidence on the presence of modes in each bin. This methodology highly depends on the arbitrary choice of the histogram bin width.

In a previous paper [42], QCH were used to estimate modes whose precision only slightly depends on the histogram granularity. Instead of choosing the "best" bin width, the naive definition of a mode (based on a supposedly continuous underlying density) has been replaced by the concept of "mode at granularity Γ". This model deals with the sparse nature of discrete random data. If Δ is the granularity of the histogram (the cardinal, or area, of the bins: $|\boldsymbol{h_k}| = \Delta$), finding a mode at granularity $\Gamma > \Delta$ amounts to finding a set $\boldsymbol{w_\Gamma}$ ($|\boldsymbol{w_\Gamma}| = \Gamma$) that locally maximizes the number of votes accumulated in it: $Nb(\boldsymbol{w_\Gamma})$. Then, the pignistic transfer is used to estimate and locally maximize this number.

A question may rise: which membership function has to be used for the $\boldsymbol{w_\Gamma}$ subset? After many tries using triangular, crisp and other membership functions of various size, we found that the crisp subset with $\Gamma = 2\Delta$ (the width of $\boldsymbol{w_\Gamma}$ is the same as the partition bin $\boldsymbol{h_k}$ one) has the best properties with respect to the pignistic transfer. Indeed, when data are uniformly spread, the estimated pdf is also uniform. For other tested configurations a complex normalizing factor was needed and the pdf estimation was less accurate. For this specific $\boldsymbol{w_\Gamma}$, it only interferes with four contiguous cells of the fuzzy partition (Fig. 8). The votes transfer procedure is simplified and a local mode position, over the four intersected histogram cells, can be literally computed. A more detailed study on quasi-continuous histograms performances and theory can be found in [41].

The local mode estimation procedure is now presented. Let $\boldsymbol{h_k}$ be the first intersected bin (from left to right), $\alpha\Delta$ be the gap between m_k (the modal value of $\boldsymbol{h_k}$) with $\alpha \in [0, 1]$ and $\boldsymbol{w}$'s lower boundary. When data are precise, $Nb(\boldsymbol{w_\Gamma}; (d_i))$ can

Please cite this article as: F. Comby, O. Strauss, Using quasi-continuous histograms for fuzzy main motion estimation in video sequence, Fuzzy Sets and Systems (2006), doi: 10.1016/j.fss.2006.09.011

be expressed as a function of α. Finding the pdf mode amounts to finding the position of $\boldsymbol{w_\Gamma}$ maximizing $Nb(\boldsymbol{w_\Gamma}; (d_i))$. An extreme value is computed locally which satisfies the following proposition:

Proposition 1. *For each subset* $\boldsymbol{w_\Gamma}$ *satisfying* $\boldsymbol{w_\Gamma} \subset [m_k, m_{k+3}]$ *and* $|\boldsymbol{w_\Gamma}| = 2\Delta$ *there is either a unique local solution* $\hat{\alpha} \in [0, 1]$ *such as*: *whatever be* $\alpha \in [0, 1]$, $Nb_\alpha(\boldsymbol{w_\Gamma}; (d_i)) < Nb_{\hat{\alpha}}(\boldsymbol{w_\Gamma}; (d_i))$ *or no local solution.*

Proof. Because the pdf approximation, $Nb(\boldsymbol{w_\Gamma}; (d_i))$, is a second-order polynomial function of α, its first-order derivative is a first-order polynomial function of α admitting only one root. Then, the solution if it exists, i.e. $\hat{\alpha} \in [0, 1]$, is unique. Otherwise, if $\hat{\alpha} \notin [0, 1]$ there is no local solution. □

Finding the histogram associated pdf local mode within the $[m_{k+1}, m_{k+2}]$ interval, amounts to solving $\mathrm{d}/\mathrm{d}\alpha\, Nb(\boldsymbol{w_\Gamma}; (d_i)) = 0$. Indeed, $Nb_\alpha(\boldsymbol{w_\Gamma}; (d_i))$ only depends on α. The value of $\hat{\alpha}$, if it exists (i.e. $\hat{\alpha} \in [0, 1]$), is given in Eq. (17) and depends on the accumulator values: $Acc_k, \ldots, Acc_{k+3}$.

$$\hat{\alpha} = \frac{Acc_k - Acc_{k+2}}{Acc_k - Acc_{k+1} - Acc_{k+2} + Acc_{k+3}}. \tag{17}$$

Once all local modes have been computed, the overall mode of the histogram is set as the position of the maximum of all local modes $Nb_{\hat{\alpha}}(\boldsymbol{w_\Gamma}; (d_i))$.

When the data are imprecise, the histogram is also imprecise and $Nb(\boldsymbol{h_k}; (\boldsymbol{d_i}))$ is only known by its framing: $[\underline{Nb}(\boldsymbol{w}; (\boldsymbol{d_i})), \overline{Nb}(\boldsymbol{w}; (\boldsymbol{d_i}))]$. The only solution we know to take a decision on $Nb(\boldsymbol{h_k}; (\boldsymbol{d_i}))$ is to reason on the midpoint of its interval. With the procedure described above, it amounts in searching α verifying $\mathrm{d}/\mathrm{d}\alpha\, Nb(\boldsymbol{w}; (\boldsymbol{d_i})) = 0$ with $Nb(\boldsymbol{w}; (\boldsymbol{d_i})) = (\underline{Nb}(\boldsymbol{w}; (\boldsymbol{d_i})) + \overline{Nb}(\boldsymbol{w}; (\boldsymbol{d_i})))/2$.

3.6. Quasi-continuous histograms in 2 and N-dimension

To deal with computer vision problems, this article briefly presents the 2-D extension of QCH. The N-D generalization is easy to understand and will not be presented in this paper. When the distribution is bi-dimensional, QCH is also bi-dimensional. Triangular fuzzy cells are changed in pyramidal fuzzy 2-D cells considering the t-norm min [13]. Such a partition is illustrated in Fig. 9.

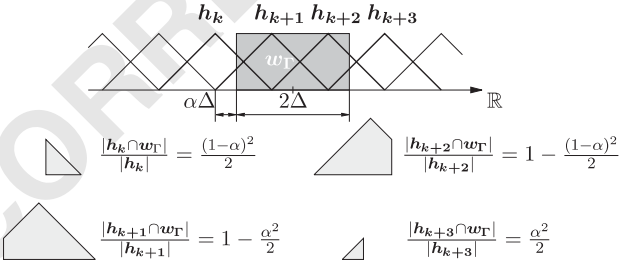

Fig. 8. The set $\boldsymbol{w_\Gamma}$ with $\Gamma = 2\Delta$ only interferes with the cells $\boldsymbol{h_k}, \boldsymbol{h_{k+1}}, \boldsymbol{h_{k+2}}, \boldsymbol{h_{k+3}}$. The cardinal (area) of their intersection with $\boldsymbol{w_\Gamma}$ is used to compute $Nb(\boldsymbol{w_\Gamma}; (d_i))$.

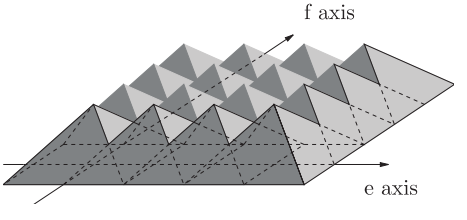

Fig. 9. 2-D Fuzzy partition.

Please cite this article as: F. Comby, O. Strauss, Using quasi-continuous histograms for fuzzy main motion estimation in video sequence, Fuzzy Sets and Systems (2006), doi: 10.1016/j.fss.2006.09.011

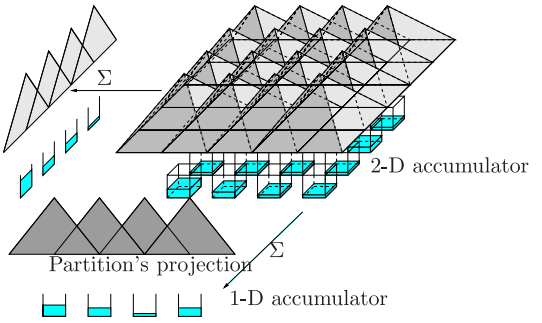

Fig. 10. 2-D fuzzy partition projection and its associated accumulator.

Formulas (7) and (8) are replaced by Formulas (18) and (19),

$$\overline{Acc_{k,l}} = \sum_{i=1}^{N}\sum_{j=1}^{M} \Pi(\boldsymbol{h}_{k,l}; \boldsymbol{d}_{i,j}), \tag{18}$$

$$\underline{Acc_{k,l}} = \sum_{i=1}^{N}\sum_{j=1}^{M} N(\boldsymbol{h}_{k,l}; \boldsymbol{d}_{i,j}), \tag{19}$$

where $\boldsymbol{h}_k$ and $\boldsymbol{h}_l$ are the 1-D projections of the cell $\boldsymbol{h}_{k,l}$ on the "e" and "f" axes, $\Pi(\boldsymbol{h}_{k,l}; \boldsymbol{d}_{i,j}) = \min(\Pi(\boldsymbol{h}_k; \boldsymbol{d}_i); \Pi(\boldsymbol{h}_l; \boldsymbol{d}_j))$ and $N(\boldsymbol{h}_{k,l}; \boldsymbol{d}_{i,j}) = \min(N(\boldsymbol{h}_k; \boldsymbol{d}_i); N(\boldsymbol{h}_l; \boldsymbol{d}_j))$.

The 2-D generalization of Eq. (14) involves hard geometrical computations (intersections of volumes), thus limiting the use of pignistic transfer. We opted for a projective approach. As the 1-D mode estimation can be locally computed on four contiguous cells, the estimation of the 2-D mode is locally computed on 4×4 cells units. The mode is sought on the two 1-D local projections—following the procedure described in Section 3.5—in order to simplify the research. This procedure is illustrated in Fig. 10.

A local 2-D mode research is more or less the same—in terms of complexity—as two 1-D local mode researches. The loss of information due to the projections was evaluated and resulted in 0.15% noise in the vote number estimation [8]. The extension to N-D QCH follows the same logic. However, graphical representation becomes impossible as soon as $N > 2$.

4. Motion estimation

Our motion estimation method is based on a combined fuzzy-statistical process that uses a new way of modeling image representation. This new model is presented in the first part of this chapter. The second part introduces a new matching process according to this image representation. The third part is dedicated to the imprecise transformation principle. The fourth part details the main motion estimation. Finally, the motion estimator behavior in different configurations is illustrated with a few examples.

4.1. Linguistic representation of an image

In all methods presented in the introduction, the gray level distribution is used as a direct measurement of the supposed continuous image photo-density distribution. The correlation-based methods assume that local patterns are retained through the image sequence, while gradient-based methods assume that a local brightness distribution is retained. Although mathematical quantitative modeling has historically emerged as the most convenient form to represent causal interactions, it has gradually become clear that processes based on semantic relations are more robust regarding causal modeling [2].

The approach presented here is based on a very simple symbolic hypothesis on modeling a kind of human perception of optical flow. It assumes that the photo receptive sensor performs a fuzzy (imprecise) classification, splitting the set of

Please cite this article as: F. Comby, O. Strauss, Using quasi-continuous histograms for fuzzy main motion estimation in video sequence, Fuzzy Sets and Systems (2006), doi: 10.1016/j.fss.2006.09.011

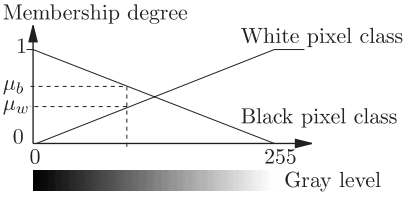

Fig. 11. Fuzzy membership function of pixel classes.

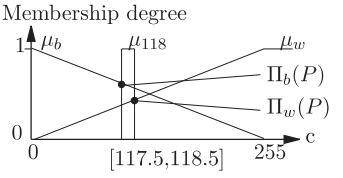

Fig. 12. The gray level space digitization effects on a 118 gray level valued pixel belonging to the white and black pixels classes.

pixels into two dual classes: bright (white) pixels and dark (black) pixels. This classification is assumed to be retained when the camera is moving. The middle gray pixels are the least reliable.

This modeling is weak and simple. It is very easy to obtain a fuzzy classification by using a linear fuzzification operator (Fig. 11).

After classification, each pixel (P) is represented by its membership degree to each class ($\mu_{\mathrm{w}}(P)$ and $\mu_{\mathrm{b}}(P)$). White and black classes are dual, i.e. $\mu_{\mathrm{w}}(P) = 1 - \mu_{\mathrm{b}}(P)$.

In fact, the gray level of each pixel is an imprecise quantity due to digitization. The pixel gray level is only known within an interval and may be characterized by its membership function $\mu_{\mathrm{gl}(P)}$. Therefore, in order to take the gray level digitization into account, the membership function has to be replaced by the possibility of each pixel being black ($\Pi_{\mathrm{b}}(P)$) or white ($\Pi_{\mathrm{w}}(P)$), with:

$$\Pi_{\mathrm{b}}(P) = \sup_c(\min(\mu_{\mathrm{b}}(c), \mu_{\mathrm{gl}(P)}(c))), \tag{20}$$

$$\Pi_{\mathrm{w}}(P) = \sup_c(\min(\mu_{\mathrm{w}}(c), \mu_{\mathrm{gl}(P)}(c))) \tag{21}$$

with c being the gray level axis, $\mu_{\mathrm{gl}(P)}$ the membership function of pixel P's gray level (Fig. 12). An illustration of this phenomenon is given in Fig. 12 for a pixel whose gray level is 118. In fact its gray level belongs to the interval [117.5, 118.5]. Duality between classes is then expressed by a weaker relation: $1 - \Pi_{\mathrm{b}}(P) \leqslant \Pi_{\mathrm{w}}(P)$.

When a multi-resolution process is needed, either to reduce computation time or improve performance of an image processing algorithm, linguistic representation aims to retain, as much as possible, all information about the pixel classification. If $\Pi^n_{\mathrm{b}}(P_i)$ (resp. $\Pi^n_{\mathrm{w}}(P_i)$) is the possibility that pixel P_i could be black (resp. white) at resolution n, then $\Pi^{n+1}_{\mathrm{b}}(P_i) = \sup_k(\min(\Pi^n_{\mathrm{b}}(P_k), \Pi(P_i; P_k)))$. Classical multi-resolution methods are based either on filtering the image via a kernel, using wavelets or by reducing the size of an image via averaging of pixel units [11,38]. These methods assume that gray-level variations on the image are smooth. Violation of this hypothesis introduces a blurring effect on the object boundaries. The linguistic multi-resolution process is an hyper-careful method aimed at minimizing the loss of information without any assumption about the a priori pixel gray level distribution.

4.2. Linguistic matching

The linguistic matching process assumes that the fuzzy classification is retained between two consecutive images in a video sequence.

Definition 1. A pixel P_i of an image can be matched with a pixel P_j in another image if P_i and P_j belong to the same class of pixels: i.e. P_i *and* P_j belong to the white pixel class *or* P_i *and* P_j belong to the black pixel class.

Please cite this article as: F. Comby, O. Strauss, Using quasi-continuous histograms for fuzzy main motion estimation in video sequence, Fuzzy Sets and Systems (2006), doi: 10.1016/j.fss.2006.09.011

This proposal prompts us to evaluate the matching bipolar potential between P_i and P_j, with:

$$\Pi_R(P_i; P_j) = \max(\min(\mu_w(P_i); \mu_w(P_j)); \min(\mu_b(P_i); \mu_b(P_j))) \tag{22}$$

representing how much it is possible to match P_i and P_j when only the gray level classification is considered; and

$$\Pi_{\overline{R}}(P_i; P_j) = \max(\min(\mu_w(P_i); \mu_b(P_j)); \min(\mu_b(P_i); \mu_w(P_j))) \tag{23}$$

representing how much it is possible to not match P_i and P_j considering only the gray level classification. According to the bipolar modeling, $\Pi_R(P_i, P_j) \geqslant 1 - \Pi_{\overline{R}}(P_i, P_j) = N_R(P_i, P_j)$. The upper and lower boundaries of the matching probability between P_i and P_j are respectively: $\Pi_R(P_i; P_j)$ and $\Pi_{\overline{R}}(P_i; P_j)$.

4.3. Imprecise transformation

Our estimation process is based on a sampled parametered representation of pixel displacement. To simplify the process explanation, the apparent motion model is assumed to be characterized by two translations along the (x, y) axes and a rotation around the z axis $A = [t_x, t_y, \alpha]^T$. According to this model, when a pixel P is moved with respect to these parameters, it becomes P'.

$$P' = R_\alpha(P - T) = f(A, P), \tag{24}$$

where R_α is the α angle rotation matrix and $T = [tx, ty]^T$.

Classical statistical processes try to keep track of quantization by assuming some properties about the statistical distribution of the sampled information. Such a modeling generally improves the estimation precision. However, the modeling robustness is low. Conversely, set-theoretic reasoning focuses on robustness. Each sample is represented by a set (crisp or fuzzy) and no assumption about the distribution is made.

Therefore, we propose to take image modeling into account by considering each pixel as a fuzzy box (Fig. 13), i.e. a fuzzy quantity of $\mathbb{R}^2$. Each pixel of an image I is represented by its coordinates (i, j) that map real positions x_i, y_j in the image. To avoid suppositions in the pixel model, a mono-modal fuzzy set with a rectangular support is used.

Due to parameter space quantization, the same modeling has to be used for these parameters. Then, a fuzzy box will represent the domain of each variable. As $\boldsymbol{tx}, \boldsymbol{ty}, \boldsymbol{\alpha}$ are sets, they can be defined by their mode (tx_0, ty_0, α_0) and support $(tx \in [tx_0 - \Delta_{tx}, tx_0 + \Delta_{tx}], ty \in [ty_0 - \Delta_{ty}, ty_0 + \Delta_{ty}], \alpha \in [\alpha_0 - \Delta_\alpha, \alpha_0 + \Delta_\alpha])$. $A = (t_x, t_y, \alpha)$ has to be considered as a set and is noted $\boldsymbol{A} = [\boldsymbol{tx}, \boldsymbol{ty}, \boldsymbol{\alpha}]^T$. The point to point f function in Eq. (24) is converted to a set-theoretic function $\boldsymbol{f}$ with:

$$\boldsymbol{P'} = \boldsymbol{f}(\boldsymbol{A}, \boldsymbol{P}). \tag{25}$$

Fig. 14 illustrates the effects of motion parameter imprecision on P'.

Therefore, using the extension principle [13], Eq. 25 becomes:

$$\mathcal{P}' = \boldsymbol{f}(\mathcal{A}, \mathcal{P}) \tag{26}$$

with $\mathcal{X}$ being the fuzzy quantity associated to set $\boldsymbol{X}$.

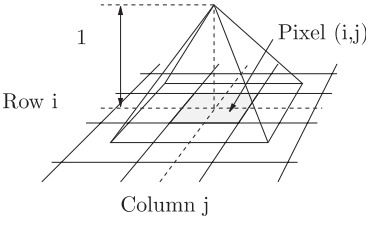

Fig. 13. Fuzzy quantity for a pixel $\mathcal{P}_1$.

Please cite this article as: F. Comby, O. Strauss, Using quasi-continuous histograms for fuzzy main motion estimation in video sequence, Fuzzy Sets and Systems (2006), doi: 10.1016/j.fss.2006.09.011

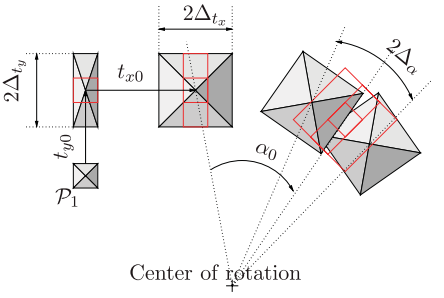

Fig. 14. Imprecise transformation of pixel P.

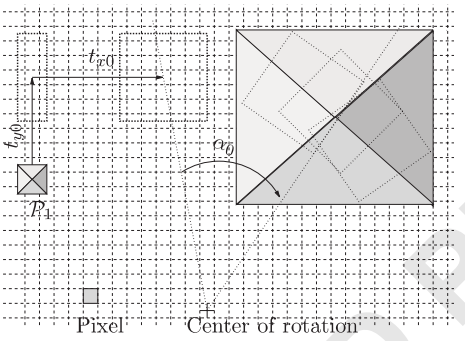

Fig. 15. Fuzzy quantity derived from the variational calculus.

Different methods, derived from [13] using the extension principle allow us to compute the transformation $\mathcal{P}'$ of the fuzzy subset $\mathcal{P}$ by the imprecise transformation $\boldsymbol{f}$. However these methods are often computationally time consuming. It is more convenient to use techniques developed in the interval analysis process [27]. A pessimistic fuzzy quantities calculation technique can be used to compute the fuzzy quantity $\mathcal{P}'$, assuming that the mode of $\mathcal{P}'$ is the image of the mode of $\mathcal{P}$ by $\boldsymbol{f}$ and using variational calculus to compute the support of $\mathcal{P}'$. Fig. 15 illustrates the results of the computation of the $\mathcal{P}'$ support.

Remark 3. It is easy to generalize this principle to more complex motion model. For example if an affine motion model using 6 parameters is considered, Eq. (24) will be transformed in

$$P' = \begin{pmatrix} x' & y' \end{pmatrix}^{\mathrm{T}} = \begin{pmatrix} a & b & c \\ d & e & f \end{pmatrix} \begin{pmatrix} x & y & 1 \end{pmatrix}^{\mathrm{T}}.$$

Also each parameter $(a, b, \ldots, f)$ has to be considered as a set $(\boldsymbol{a}, \boldsymbol{b}, \ldots, \boldsymbol{f})$ due to the parameter space discretization.

4.4. Main apparent motion estimation

Apparent motion estimation aims at finding the parameter values representing the most frequent displacement in the image (according to the displacement model). The QCH formalism presented in Section 3 will be used to perform this estimation.

Let (A_k) with $k = 1$ to p be the kth fuzzy set of parameters representing a displacement. The accumulation process is based on the following rule:

Definition 2. A pixel P_1 from image I_1 is said to have a possible displacement that belongs to the displacement set characterized by $\boldsymbol{A_k}$ if a pixel P_2 belongs to $\boldsymbol{f}(\mathcal{P}_1, \mathcal{A}_k)$ and matches P_1.

Please cite this article as: F. Comby, O. Strauss, Using quasi-continuous histograms for fuzzy main motion estimation in video sequence, Fuzzy Sets and Systems (2006), doi: 10.1016/j.fss.2006.09.011

Since the process is bipolar, the dual rule has to be expressed:

Definition 3. A pixel P_1 from image I_1 is said to have no possible displacement that belongs to the displacement set characterized by $\boldsymbol{A_k}$ if no pixel P_2 belongs to $\boldsymbol{f}(\mathcal{P}_1, \mathcal{A}_k)$ and matches P_1.

We will use the necessity of displacement instead of the impossibility of displacement. According to linguistic matching and imprecise transformation, these rules can be written as

$$\begin{aligned} Vote_{\text{upper}\,P_1}(\mathcal{A}_k) &= \sup_{P_2 \in I_2} (\min(\Pi(\mathcal{P}_1'; \mathcal{P}_2), \Pi_R(P_1; P_2))), \\ Vote_{\text{lower}\,P_1}(\mathcal{A}_k) &= 1 - \sup_{P_2 \in I_2} (\min(N(\mathcal{P}_1'; \mathcal{P}_2), N_R(P_1; P_2))) \end{aligned} \tag{27}$$

with

$$\begin{aligned} N(\mathcal{P}_1'; \mathcal{P}_2) &= \inf_{P2 \in I} (\max(\mu_{\mathcal{P}_1'}(P), 1 - \mu_{\mathcal{P}_2}(P))), \\ \Pi(\mathcal{P}_1'; \mathcal{P}_2) &= \sup_{P2 \in I} (\inf(\mu_{\mathcal{P}_1'}(P), \mu_{\mathcal{P}_2}(P))), \end{aligned} \tag{28}$$

where I is the image, $P \in \mathbb{R}^2$, $\mu_{\mathcal{P}}$ is the membership function associated to the fuzzy quantity $\mathcal{P}$.

When a specific motion applied to a pixel leads it out of the picture boundaries, the gray level value of such a moved pixel is unknown. In correlation-based techniques such a pixel is usually ignored or set to an arbitrary value (0 or 255). In fact, its gray level is unknown within the interval [0, 255]. According to the pixel representation presented here, $\Pi_{\text{b}}(P)$ and $\Pi_{\text{w}}(P)$ are set to 1. This represents the total uncertainty about the pixel gray level. Such pixels will thus not add arbitrary information, but the fact that they are unknown is integrated in the estimation process.

The computation complexity of $N(\mathcal{P}_1'; \mathcal{P}_2)$ and $\Pi(\mathcal{P}_1'; \mathcal{P}_2)$ can be reduced using 1-D projections of the fuzzy quantities (Fig. 16), as

$$\begin{aligned} N(\mathcal{P}_1'; \mathcal{P}_2) &= \min(Nx(\mathcal{P}_1'; \mathcal{P}_2), Ny(\mathcal{P}_1'; \mathcal{P}_2)), \\ \Pi(\mathcal{P}_1'; \mathcal{P}_2) &= \min(\Pi x(\mathcal{P}_1'; \mathcal{P}_2), \Pi y(\mathcal{P}_1'; \mathcal{P}_2)), \end{aligned} \tag{29}$$

where $\Pi x(\mathcal{P}_1'; \mathcal{P}_2)$ is the degree of possibility of matching $\mathcal{P}_1'$ and $\mathcal{P}_2$ projections on the x-axis. As the 2-D-fuzzy quantities are defined as the Cartesian product of two 1-D-fuzzy quantities, there is no loss of accuracy while using the projections.

Each possible vote (resp. necessary) are accumulated in the upper (resp. lower) accumulator of the QCH built on the motion parameters space. Finally searching for the main apparent motion amounts to searching for the main mode

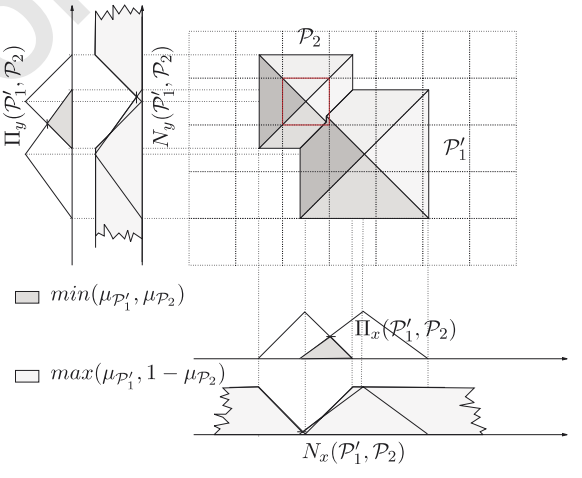

Fig. 16. Computation of the compatibility between $\mathcal{P}_1'$ and $\mathcal{P}_2$ using their projections on the X and Y axes.

Please cite this article as: F. Comby, O. Strauss, Using quasi-continuous histograms for fuzzy main motion estimation in video sequence, Fuzzy Sets and Systems (2006), doi: 10.1016/j.fss.2006.09.011

of the QCH built on the motion parameters. This search is performed with the mode estimation method presented in Section 3.5.

5. Results

The algorithm performances are now illustrated through simulated and real video sequences. The aim of simulated sequences is to evaluate the algorithm's performances in terms of accuracy. Real sequences also present some interesting difficulties. Actually many hypotheses are violated, like

- The scene is not planar (it presents large depth variations with respect to the distance between the scene and the camera).
- The scene brightness is not constant (which is often true with outdoor videos or with web-cams as they are equipped with an automatic gain control).
- Parasite motions alter the main motion (small objects have their own motion and generate local concealment of the "background'').
- The motion to be estimated does not exactly match the motion model used.

The motion estimation process has to be robust to deal with these perturbations.

5.1. Results on simulated image sequences

Simulated sequences are generated from a single 1125 × 745 pixels image. Small images (80 × 60 pixels) are extracted from it with known real (not integer) displacements between them. These displacements are confined to the parametric space range.

5.1.1. Ideal case

This section presents some results obtained with simulated sequences. The performances of the algorithm are compared with those obtained with state of the art methods. The optical flow is computed with the robust multi-resolution algorithm presented in [31] but with no illumination compensation.

The first case presented is optimal, where all working hypotheses are satisfied because of the image sequence generation (planarity of the scene, constant global illumination and no parasite motion). The test involves generating 100 images (frame size: 80 × 60) with a random bounded displacement and estimating the motion between each pair of images. The parameter boundaries and research area were defined as: Tx and $Ty \in [-4, 4]$ and $\alpha \in [-10, 10]$. The discretization step for the translations is 1 pixel and 2.5° for rotations. Table 3 shows some statistics on the difference between reference and estimated motion parameters for correlation-based, optical flow and QCH methods.

The first point to note is that the estimation is more precise for optical flow and QCH than correlation based-methods. In fact the precision of correlation-based methods depends on the motion parameter space sampling step. This effect is

Table 3
This table presents statistics on motion parameters deviation (between source displacement and estimated one) in the ideal case for a 100 images sequence

Error	Tx (pixels)			Ty (pixels)			α (degrees)		
	Mean	Max	σ	Mean	Max	σ	Mean	Max	σ
SAD	0.68	1.92	0.48	0.56	1.69	0.4	0.77	2.14	0.58
ZSAD	0.53	1.72	0.45	0.52	1.69	0.4	0.62	1.36	0.42
SSD	0.79	2.58	0.64	0.61	1.75	0.47	0.87	2.63	0.67
ZSSD	0.78	2.58	0.55	0.57	1.69	0.41	0.8	2.14	0.61
NCC	0.82	2.58	0.63	0.58	1.69	0.41	0.87	2.63	0.67
ZNCC	0.75	2.58	0.57	0.57	1.69	0.41	0.8	2.14	0.61
CENSUS	0.62	2.74	0.58	0.56	1.33	0.34	1.12	9.23	1.66
OF	0.47	1.57	0.41	0.36	0.98	0.28	0.11	1.04	0.19
QCH	0.42	1.62	0.45	0.34	1.05	0.29	0.28	0.68	0.17

Mean (resp. Max) is the mean (resp. maximum) value of the absolute error. σ is the standard deviation of the absolute error.

Please cite this article as: F. Comby, O. Strauss, Using quasi-continuous histograms for fuzzy main motion estimation in video sequence, Fuzzy Sets and Systems (2006), doi: 10.1016/j.fss.2006.09.011

Fig. 17. Original image (left) and the same image with each gray level decreased of 40 (right).

Table 4
Statistics on motion parameters errors with an illumination variation for a 100 images sequence

Error	*Tx* (pixels)			*Ty* (pixels)			α (degrees)		
	Mean	Max	σ	Mean	Max	σ	Mean	Max	σ
SAD	0.89/0.7	2.58/2.25	0.64/0.52	0.57/0.51	1.69/1.52	0.4/0.41	0.74/0.72	2.14/1.79	0.56/0.44
ZSAD	0.78/0.7	2.37/2.25	0.6/0.52	0.53/0.51	1.69/1.52	0.4/0.42	0.62/0.72	1.36/1.79	0.41/0.44
SSD	0.82/0.77	2.58/2.5	0.65/0.56	0.62/0.8	1.75/1.82	0.46/0.44	0.87/1.08	2.63/2.4	0.67/0.67
ZSSD	0.82/0.74	2.58/2.5	0.61/0.61	0.67/0.8	1.75/1.82	0.47/0.44	0.88/1.08	2.63/2.4	0.68/0.67
NCC	0.85/0.77	2.58/2.5	0.64/0.6	0.61/0.8	1.75/1.82	0.47/0.44	0.87/1.08	2.63/2.4	0.67/0.67
ZNCC	0.79/0.77	2.58/2.5	0.62/0.6	0.61/0.8	1.75/1.82	0.47/0.44	0.88/1.08	2.63/2.4	0.68/0.67
CENSUS	0.62/0.59	2.74/2.25	0.58/0.53	0.56/0.5	1.33/1.32	0.34/0.37	1.12/0.77	9.23/2.33	1.66/0.5
OF	4.96/1.75	10.3/6.5	2.86/1.78	8.01/2.67	19.19/17.17	3.67/4.48	2.87/1.01	6.64/4.31	1.64/1.13
QCH	0.79/0.49	2.56/1.38	0.62/0.44	0.46/0.35	1/1.04	0.32/0.28	0.52/0.43	1.63/1.14	0.41/0.31

Mean (resp. Max) is the mean (resp. maximum) value of the absolute error. σ is the standard deviation of the absolute error. The first number is for a global variation of −40 gray level on one image out of two, the second for a local variation of −40 gray level on a restricted zone on each image.

more significant for rotation estimation where the sampling step is larger. QCH method is also sensitive to this sampling, but using a fuzzy partition relaxes this constraint and increases the mode estimation precision. Moreover, when no mode is found on the histogram, QCH algorithm can provide an error message instead of delivering an erroneous result as correlation-based methods do. In this sequence, the error on Ty is less important than on Tx because of the geometry of the scene. The major drawback of the QCH algorithm is its computation time: it takes 28.1 s to compute the main motion for a pair of images. To compare, the estimation only takes 3.1 s for the SAD algorithm and 0.2 s for the optical flow algorithm. However this point will be discussed in the conclusion.

5.1.2. Robustness tests

As presented in the introduction, some disruptions can alter the motion parameter estimation. The following examples illustrate the robustness of our approach.

The first case involves modifying the brightness of one image in each pair of images. This phenomenon often occurs in outdoor sequences where there is no control on the light source. This also occurs when the light source used is a fluorescent light (in submarine sequences, in office environment, etc.). The light intensity varies asynchronously with the image acquisition device which results in global illumination variation. In the example presented, all pixel gray level were decreased of 40 on each second image. A saturation effects occurs as black pixels (gray level equals 0) remain black and are not modified. The effects of such a variation are illustrated in Fig. 17.

Table 4 shows the motion parameters estimation errors for the different approaches.

The optical flow-based algorithm (without light variation compensation process) is obviously unable to estimate the motion. In fact, the main working hypothesis is transgressed, thus inducing estimation errors. This perturbation penalizes less correlation-based methods. However, the correlation score is affected by illumination variations. The estimation reliability threshold has to be changed depending on the kind of picture used. The census transform is almost not disrupted since a global brightness change does nearly not affect the pixel intensity order (which is not true for a local brightness change). Even if the errors increase slightly, QCH provides a good estimation of the motion parameters.

Please cite this article as: F. Comby, O. Strauss, Using quasi-continuous histograms for fuzzy main motion estimation in video sequence, Fuzzy Sets and Systems (2006), doi: 10.1016/j.fss.2006.09.011

Table 5
Statistics on motion parameters errors for a 100 images sequence with an object covering 15% of the image and moving independently

Error	*Tx* (pixels)			*Ty* (pixels)			α (degrees)		
	Mean	Max	σ	Mean	Max	σ	Mean	Max	σ
SAD	0.41	0.99	0.29	0.32	1.02	0.26	0.76	1.47	0.37
ZSAD	0.41	0.99	0.29	0.32	1.02	0.26	0.76	1.47	0.37
SSD	0.52	1.66	0.4	0.56	1.87	0.44	0.94	2.03	0.53
ZSSD	0.52	1.66	0.4	0.56	1.87	0.44	0.94	2.03	0.53
NCC	0.52	1.66	0.4	0.57	1.87	0.44	0.94	2.03	0.53
ZNCC	0.43	1.16	0.31	0.50	1.87	0.44	0.92	2.03	0.52
CENSUS	0.91	4.74	1.15	0.75	4.7	0.99	1.22	10.31	1.78
OF	0.34	4.25	0.75	0.29	1.14	0.27	0.21	0.89	0.26
QCH	0.25	0.96	0.22	0.3	1.11	0.25	0.44	1.27	0.3

Mean (resp. Max) is the mean (resp. maximum) value of the absolute error. σ is the standard deviation of the absolute error.

Tests with local intensity variations have also been performed. These tests consist in increasing the gray levels of a 40 pixel diameter circle by 40. Moreover, this pattern randomly moves on the image. Since all algorithms estimate main motion (estimation based on a large number of pixels), a local intensity variation does not cause a failure of the estimators. with respect to the ideal case, optical flow algorithm is the most affected. Correlation-based methods are little bit affected, and QCH algorithm presents the best results.

Another kind of perturbation is the presence of parasite motions, i.e. objects in the scene having their own motion (different from the main motion). To perform this test, we overlaid a small pattern on the image. This pattern covers about 15% of the image and randomly moves on it. Table 5 shows the motion parameters estimation errors. In this experiment, some errors are smaller than in previous estimations because the parasite pattern is mainly overlaid on a relatively homogeneous zone, thus generating uncertainty in the motion estimation. QCH and optical flow algorithms provide the best motion parameters estimation. The census transformation is especially disrupted as the order of pixels is modified by the parasite pattern visible on the sequence. This introduces substantial error in the motion parameter estimation.

It is noticeable that in all cases the QCH provides a good motion parameters estimation. This is not the case for optical flow algorithm when the sequence presents some illumination variations. Correlation-based methods seems to work in almost all cases. However, their performances are linked to the motion parameters space sampling. Robust correlation methods using census transform are unaffected by global illumination variations but are very sensitive to occlusions modifying the relative pixel intensity order.

5.2. Results on real image sequences

The following tests were performed on real image sequences. They illustrate the robustness of the QCH algorithm when the working hypotheses are not fulfilled. However, the real displacements were unknown, thus the graphical consistency of the reconstructed image was the only criterion available to assess the estimation quality.

The first test uses the sequence of houses (150 frames of 352 × 240 pixels) where the camera motion is mainly a translation to the left. This scene has major depth variations between the foreground (tree) and the background (houses). Fig. 18 shows two images (left and center) of the sequence used for the motion estimation. The third image represents the superposition of these two images according to the motion estimation method. A transparency effect was added to show the effects of different motions due to depth variations. The main motion is assigned to the main "layer'' in the image, corresponding to the houses and a part of the garden. The tree is not well superposed because its motion does not match the main motion. This example illustrates that even if the planarity of the scene is not fulfilled, the main motion estimation with the QCH is reliable. The second example involves a pair of images of a stone wall (issued from a sequence of 30 images of 160 × 120 pixels). This test was performed to illustrate the robustness concerning illumination variation. The scene is supposed to be plane, but the delay between the two shots was long enough for the illumination to change (Fig. 19).

Please cite this article as: F. Comby, O. Strauss, Using quasi-continuous histograms for fuzzy main motion estimation in video sequence, Fuzzy Sets and Systems (2006), doi: 10.1016/j.fss.2006.09.011

Fig. 18. Two images of the houses and tree sequence (top left and right) and their superposition according to the motion estimation (middle). The fourth image (bottom) presents the mosaic of all images according to the motion estimation.

Fig. 19. Two images of a stone wall (top left and right) with a variation in illumination and their superposition according to the motion estimation (bottom).

The stones seem to fit between the two images even with the illumination variation. This illustrates the robustness of the QCH algorithm with respect to non-conservation of global brightness.

The last example—to test the robustness with respect to secondary motion—is a short sequence of four 160×120 images (Fig. 20 top) where the main motion on the image is due to left to right camera motion. A character is moving in the opposite direction on the sequence, thus generating parasite motion. The superposition of these four images according to the motion (Fig. 20 bottom) indicates that the estimation does not seem to be altered by this secondary motion. This illustrates the robustness of the estimation concerning parasite motion.

The last experiment involves a camera describing a closed loop trajectory on a 40 images sequence (10 cm left horizontal translation followed by a 10 cm right horizontal translation). The scene observed was far enough to be considered as a plane surface. There was no significant light variation during the experimentation. Fig. 21 presents the frame number on the abscissa and the accumulated translation estimations on the ordinate. As it could be expected the SAD algorithm presents a significant divergence (2 pixels) linked to the motion parametric space sampling. Indeed, all errors due to estimated parameters truncation are accumulated. Optical flow algorithm also presents a small divergence (0.65 pixel). QCH algorithm almost does not diverge: only 9.65×10^{-3} pixel.

Please cite this article as: F. Comby, O. Strauss, Using quasi-continuous histograms for fuzzy main motion estimation in video sequence, Fuzzy Sets and Systems (2006), doi: 10.1016/j.fss.2006.09.011

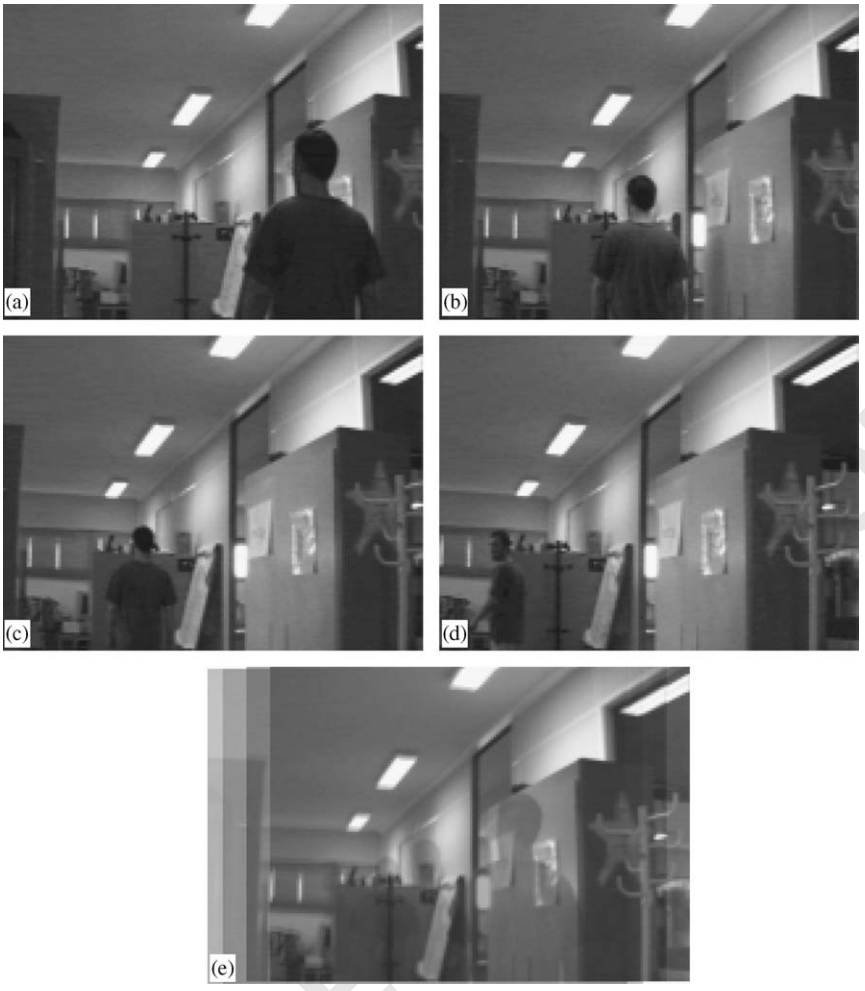

Fig. 20. Four images of the inside laboratory sequence (top and middle) with a character moving in front of the camera and their superposition according to the motion estimation (bottom).

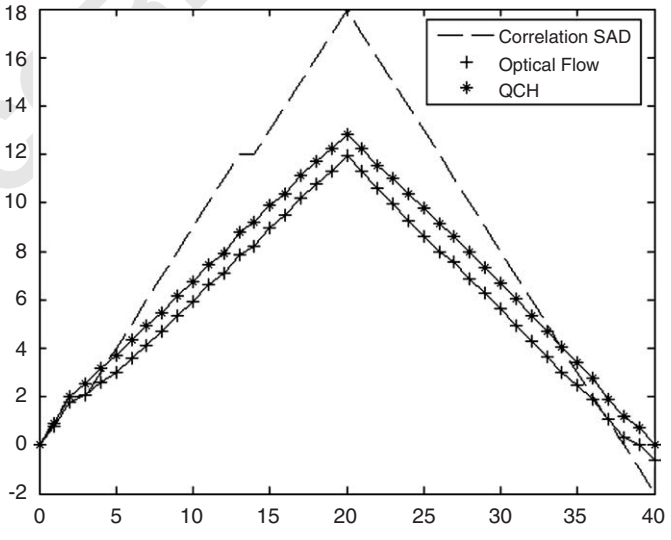

Fig. 21. Accumulation of estimated translations during the closed loop motion for SAD, OF and QCH algorithms.

Please cite this article as: F. Comby, O. Strauss, Using quasi-continuous histograms for fuzzy main motion estimation in video sequence, Fuzzy Sets and Systems (2006), doi: 10.1016/j.fss.2006.09.011

6. Summary

In this paper, a new method was introduced for main motion estimation in video sequences. This estimation is based on fuzzy modeling of the pixel gray level and uses both quasi-continuous histograms (QCH) and possibility theories.

This method partially copes with classical issues in the motion estimation process, such as the small displacement assumption and texture-linked constraints. A motion model and discretization of the motion parameter space is needed. However, using QCH enables a relatively natural interpolation, and leads to an estimation that is less sensitive to parameter space discretization.

Moreover, the most positive point concerns data contamination. Using a fuzzy model of the pixel gray level appears to be robust. Global, or local illumination variations actually do not cause failure of the estimation process. The algorithm is also robust to outliers motions, i.e. motions that differ from the main motion. In fact, even if our algorithm is not the most precise in all configurations tested, it was always able to provide a good motion estimation. This was not the case for correlation-based methods nor optical flow ones. This opens a promising way for motion estimation that needs to be further investigated.

Another positive feature of the method is that it gives an estimation of motion along with a confidence measure of this estimation. Indeed, the gap between the lower and upper accumulators is linked to this confidence measure. The greater the distance between the accumulators, the less significant the estimation is. Unlike correlation-based methods, the estimation relevance threshold is set by the data.

However, this motion estimation process has its drawbacks. First, the computing time is quite long since loops are intertwined in the algorithm. Studies are currently under way to improve this. At present, only the algorithm for two translations has been modified. It involves reasoning on integer motions to ease and allow a pre-computing of the compatibility measures (possibility and necessity). This reduces the computation time to 0.2 s for a pair of images. This process needs to be generalized for more complex motions especially those including rotations. In this case, one of the next steps of the motion estimation process will involve improving the motion model. This will require more tests on the influence of the projection algorithm for a parametric space of more than three dimensions. Using a multi-resolution process to speed the motion estimation is also envisaged. Even if our algorithm is time consuming, using QCH for video post treatments is still possible: for example for mosaicing.

As the estimation is based on a polling scheme, the overlapping rate between two images has to reach at least 75% to guarantee the estimation success. Otherwise the number of significant votes would be too small to obtain a reliable motion estimation.

An arbitrary research area for the motion model parameters should eventually be defined and requires a limitation of the estimated motion. However, this kind of process is frequently used in many applications, such as mobile robotics, when a motion prediction is available.

References

[1] P. Ashwanden, W. Guggenbühl, Experimental results from a comparative study on correlation-type registration algorithms, Robust Comput. Vision (1993) 268–289.
[2] E. Benoit, L. Foulloy, Symbolic sensors, Proc. Eighth Internat. Symp. on Artificial Intelligence Based Measurement and Control (AIMaC'91), vol. 1, 1991, pp. 131–136.
[3] M. Bennamoun, J. Banks, P. Corke, Fast and robust stereo matching algorithms for mining automation, Proc. JAF 97, vol. 1, November 1997, pp. 139–149.
[4] J.C. Bezdek, Pattern Recognition with Fuzzy Objective Function Algorithms, Plenum Press, New York, 1981.
[5] D.N. Bhat, S.K. Nayar, Motion estimation using ordinal measures, in: Proc IEEE Conf. on Computer Vision and Pattern Recognition, San Juan, Puerto Ricco, June 1997, pp. 982–987.
[6] A. Branca, G. Cicirelli, E. Stella, A. Distante, Mobile vehicles egomotion estimation from time varying image sequences, in: Proc. IEEE Internat. Conf. on Robotics and Automation, Albuquerque, New Mexico, April 1997, pp. 1886–1891.
[7] T. Brox, A. Bruhn, N. Papenberg, J. Weickert, High accuracy optical flow estimation based on a theory for warping, Proc. Eighth Euro. Conf. on Computer Vision, vol. 4, 2004, pp. 25–36.
[8] F. Comby, Estimation du movement apparent majoritaire dans une séquence video par accumulation de votes bimodaux sur un histogramme approché, Ph.D. Thesis, Université Montpellier II, Montpellier, France, décembre 2001.
[9] F. Comby, O. Strauss, M.J. Aldon, Fuzzy approach of motion estimation, Proc. 10th IEEE Internat. Conf. on Fuzzy Systems, vol. 2, Melbourne, Australia, December 2001, pp. 549–552.
[10] D. Cox, Notes on the analysis of mixed frequency distributions, Brit. J. Math. Statist. Psych. 19 (1966) 39–47.
[11] G.M. Davis, A wavelet-based analysis of fractal image compression, IEEE Trans. on Image Process. 7 (2) (1998) 141–154.

Please cite this article as: F. Comby, O. Strauss, Using quasi-continuous histograms for fuzzy main motion estimation in video sequence, Fuzzy Sets and Systems (2006), doi: 10.1016/j.fss.2006.09.011

[12] D. Dubois, L. Foulloy, G. Mauris, H. Prades, Probability-possibility transformations, triangular fuzzy sets, and probabilstics inequalities, Reliable Comput. 10 (2004) 273–297.
[13] D. Dubois, H. Prade, Possibility Theory An Approach to Computerized Processing of Uncertainty, Plenum Press, New York, 1988.
[14] D. Dubois, H. Prade, Rough fuzzy sets and fuzzy rough sets, Internat. J. General Systems 17 (2–3) (1990) 191–200.
[15] D. Dubois, H. Prade, C. Testemale, Weighted fuzzy pattern matching, Fuzzy Sets and Systems 28 (1988) 313–331.
[16] C. Fermüller, D. Shulman, Y. Aloimonos, The statistics of optical flow, Comput. Vision Image Understanding 82 (1) (2001) 1–32.
[17] D.J. Fleet, J.L. Barron, S.S. Beauchemin, Systems and experiment: performance of optical flow techniques, Internat. J. Comput. Vision 12 (1) (1994) 43–77.
[18] A. Giachetti, Matching techniques to compute image motion, Image Vision Comput. 18 (2000) 247–260.
[19] N. Gracias, J. Santos-Victor, Automatic mosaic creation of the ocean floor, in: Proc. IEEE OCEANS'98, September 1998, pp. 257–262.
[20] R. Hartley, A. Zisserman, Multiple View Geometry, Cambridge University Press, Cambridge, MA, 2000.
[21] B.K.P. Horn, B.G. Schunck, Determining optical flow, Artif. Intelligence 17 (1981) 185–203.
[22] A.D. Jepson, D.J. Fleet, T.F. El-Maraghi, Robust online appearance models for visual tracking, Proc. IEEE Conf. on Computer Vision and Pattern Recognition, vol. 1, Kauai, December 2001, pp. 415–422.
[23] J.K. Kearnay, W.B. Thompson, D.L. Boley, Optical flow estimation: an error analysis of gradient-based methods with local optimisation, IEEE Trans. Pattern Anal. Mach. Intelligence 9 (2) (1987) 229–244.
[24] B.D. Lucas, T. Kanade, An iterative image registration technique with an application to stereo vision, in: Proc. Seventh Internat. Joint Conf. on Artificial Intelligence (IJCAI '81), Vancouver, Canada, April 1981, pp. 674–679.
[25] E. Mémin, P. Perez, Dense estimation and object oriented segmentation of the optical flow with robust techniques, IEEE Trans. on Image Process. 7 (5) (1998) 703–719.
[26] A. Mitiche, P. Bouthemy, Computation and analysis of image motion: a synopsis of current problems and methods, Internat. J. Comput. Vision 19 (1) (1996) 29–55.
[27] R. Moore, Methods and Applications of Interval Analysis, vol. 2, SIAM Studies in Applied Mathematics, Philadelphia, PA, 1979.
[28] D. Murray, A. Basu, Motion tracking with an active camera, IEEE Trans. Pattern Anal. Mach. Intelligence 16 (5) (1994) 449–459.
[29] S. Nayar, A. Karmarkar, 360 × 360 mosaics, in: Proc. IEEE Internat. Conf. on Computer Vision and Pattern Recognition, June 2000, pp. 388–395.
[30] S. Negahdaripour, Revised definition of optical flow: integration of radiometric and geometric cues for dynamic scene analysis, IEEE Trans. on Pattern Anal. Mach. Intell. 20 (9) (1998) 961–979.
[31] J.M. Odobez, P. Bouthemy, Robust multiresolution estimation of parametric motion models, J. Visual Commun. Image Representation 6 (4) (1995) 348–365.
[32] Z. Pawlak, Rough sets and decision algorithms, in: Proc. Second Internat. Conf. on Rough Sets and Current Trends in Computing, Banff, Canada, October 2000, pp. 30–45.
[33] S. Peleg, B. Rousso, A. Rav Acha, A. Zomet, Mosaicing on adaptative manifolds, IEEE Trans. on Pattern Anal. Mach. Intell. 22 (10) (2000) 1144–1154.
[34] B.W. Silverman, Density Estimation for Statistics and Data Analysis, Monographs on Statistics and Applied Probability, vol. 26, Chapman & Hall, London, 1986.
[35] A. Singh, Optical Flow Computation: a Unified Perspective, IEEE Computer Society Press, Silver Spring, MD, 1992.
[36] P. Smets, Constructing the pignistic probability function in a context of uncertainty, in: M. Henrion, R.D. Schachter, L.N. Kanal, J.F. Lemmer (Eds.), Uncertainty in Artificial Intelligence 5, Elsevier Science Publishers, North-Holland, Amsterdam, 1990, pp. 29–39.
[37] P. Smets, R. Kennes, The transferable belief model, Artif. Intelligence 66 (1994) 191–243.
[38] S. Starks, V. Kreinovich, A. Meystel, Multi-resolution data processing: it is necessary, it is possible, it is fundamental, in: Proc. Internat. Conf. on Intelligent Systems and Semiotics (ISAS'97), National Institute of Standards and Technology Publication, July 1997, pp. 145–150.
[39] C. Stiller, J. Konrad, Estimating motion in image sequences a tutorial on modeling and computation of 2-D motion, Signal Process. Mag. 16 (1999) 70–91.
[40] O. Strauss, Use the fuzzy hough transform towards reduction of the precision/uncertainty duality, Pattern Recognition 32 (11) (1999) 1911–1922.
[41] O. Strauss, Imprecise statistics with quasi-continuous histograms, LIRMM Report, January 2006.
[42] O. Strauss, F. Comby, M.-J. Aldon, Rough histograms for robust statistics, Proc. Internat. Conf. on Pattern Recognition, vol. 2, IAPR, 2000, pp. 688–691.
[43] R. Viertl, Statistical Methods for Non-Precise Data, CRC Press, Boca Raton, 1996.
[44] J. Weber, J. Malik, Robust computation of optical flow in a multi-scale differential framework, Internat. J. Comput. Vision 14 (1995) 67–81.
[45] T.H. Wonnacott, R.J. Wonnacott, Introductory Statistics for Business and Economics, Workbook, 1990.
[46] R. Zabih, J. Woodfill, Non-parametric local transforms for computing visual correspondance, in: Third Euro. Conf. on Computer Vision, Stockholm, May 1994, pp. 151–158.
[47] L. Zelnik-Manor, M. Irani, Multiple-frame estimation of planar motion, IEEE Trans. Pattern Anal. Mach. Intell. 22 (10) (2000) 1105–1116.

Please cite this article as: F. Comby, O. Strauss, Using quasi-continuous histograms for fuzzy main motion estimation in video sequence, Fuzzy Sets and Systems (2006), doi: 10.1016/j.fss.2006.09.011